Reversible Equilibrium Unfolding of Triosephosphate Isomerase from *Trypanosoma cruzi* in Guanidinium Hydrochloride Involves Stable Dimeric and Monomeric Intermediates†

María Elena Chánez-Cárdenas,‡ Gerardo Pérez-Hernández,§ Brenda Guadalupe Sánchez-Rebollar,§ Miguel Costas,|| and Edgar Vázquez-Contreras*,§

Laboratorio de Patología Vascular Cerebral, Instituto Nacional de Neurología y Neurocirugía "Manuel Velasco Suárez", México, DF, Mexico, Instituto de Química, Departamento de Bioquímica, Universidad Nacional Autónoma de México, Circuito Exterior, México, DF 04510, Mexico, and Departamento de Fisicoquímica, Facultad de Química, Universidad Nacional Autónoma de México, México, DF 04510, Mexico

Received October 29, 2004; Revised Manuscript Received May 23, 2005

ABSTRACT: The reversible guanidinium hydrochloride-induced unfolding of *Trypanosoma cruzi* triosephosphate isomerase (TcTIM) was characterized under equilibrium conditions. The catalytic activity was followed as a native homodimeric functional probe. Circular dichroism, intrinsic fluorescence, and size-exclusion chromatography were used as secondary, tertiary, and quaternary structural probes, respectively. The change in ANS fluorescence intensity with increasing denaturant concentrations was also determined. The results show that two stable intermediates exist in the transition from the homodimeric native enzyme to the unfolded monomers: one (N_2*) is a slightly more expanded, non-native, and active dimer, and the other is a partially expanded monomer (M) that binds ANS. Spectroscopic and activity data were used to reach a thermodynamic characterization. The results indicate that the Gibbs free energies for the partial reactions are 4.5 ($N_2 \leftrightarrows N_2$*), 65.8 (N_2* $\leftrightarrows$ 2M), and 17.8 kJ/mol (M $\leftrightarrows$ U). It appears that TcTIM monomers are more stable than those found for other TIM species (except yeast TIM), where monomer stability is only marginal. These results are compared with those for the guanidinium hydrochloride-induced denaturation of TIM from different species, where despite the functional and three-dimensional similarities, a remarkable heterogeneity exists in the unfolding pathways.

Triosephosphate isomerase (TIM or TPI)[1] (EC 5.3.1.1) is a homodimer that catalyzes the fifth step of glycolysis (*1*). This so-called perfect catalyst (*2*) ensures the net production of ATP in the conversion of glucose to pyruvate, and hence, it is essential for maintaining life under anaerobic conditions; for this reason, when one is dealing with important human parasites, TIM has been suggested as a good target for drug design (*3, 4*). The crystallographic structures of wild-type TIMs and engineered mutants have been determined for 14 species, from Archaea (*5*) and Bacteria (*6*−*9*) to Eukarya, including unicellular and multicellular organisms, parasites, and human (*10*−*18*). All the wild-type TIMs studied so far are homodimers, with the exception of those from *Pyrococcus woesei* and *Methanothermus fervidus*, which are homotetramers (*19*). Each TIM subunit (∼250 amino acid residues with a molecular mass near 27 kDa) folds into a $(\beta/\alpha)_8$ domain. This is the so-called "TIM barrel" structural domain that comprises or is contained in ∼10% of the known enzyme structures (*20*, *21*). In all these enzymes, the active site is located at the carboxyl termini of the closed parallel β-sheet (*22*). In TIM, the degree of amino acid sequence conservation from Archaea to Eukarya is remarkable, the sequence around the active site residue, a glutamic acid, being perfectly conserved. The catalytic residues are self-contained in each monomer, and the loops at the carboxyl termini of the barrel contain both interface and active site residues (*23*).

Taking into account TIM versatility for catalysis, the complete understanding of its catalytic mechanism, and its homodimeric nature (the simplest oligomerization model), we find this enzyme is a good candidate for improving our knowledge of protein folding and assembly and, eventually, of drug design. The TIM unfolding pathways induced by guanidinium hydrochloride (Gdn-HCl) from *Bacillus stearothermophilus* (*25*), *Thermotoga maritima* (*26*), rabbit (*27*−*29*), *Plasmodium falciparum* (*30*), *Saccharomyces cerevisiae* (*31*−*33*), *Leishmania mexicana* (*34*), and *Trypanosoma brucei* (TbTIM) (*35*) have been studied in detail. Although the equilibrium unfolding pathways of homologous TIMs

† This work was supported by Grants 40524M and 41328Q from CONACyT and Grant IN113302 from PAPIIT-UNAM. G.P.-H. and B.G.S.-R. are the recipients of postdoctoral and graduate student fellowships, respectively, from CONACyT.

* To whom correspondence should be addressed. Telephone: (5255) 56224565. Fax: (5255) 56162217. E-mail: vazquezc@servidor.unam.mx.

‡ Instituto Nacional de Neurología y Neurocirugía "Manuel Velasco Suárez".

§ Departamento de Bioquímica, Universidad Nacional Autónoma de México.

|| Departamento de Fisicoquímica, Universidad Nacional Autónoma de México.

[1] Abbreviations: TIM, triosephosphate isomerase; ANS, 1-aniline-8-naphthalenesulfonate; CD, circular dichroism; Gdn-HCl, guanidinium hydrochloride; IF, intrinsic fluorescence; λ_{max}, wavelength of maximal emission; SEC, size-exclusion chromatography.

10.1021/bi047687a CCC: $30.25
Published on Web 07/21/2005

in Gdn-HCl are different, the crystallographic three-dimensional structures of these enzymes are highly similar. On the other hand, two trypanosomatid TIMs with a percentage of identity in the primary structure of 74% (*36*) show different behavior with respect to inactivation with the same sulfhydryl reagents (*3*). The equilibrium unfolding of one of them, TbTIM (*35*), is complex and irreversible. In this context, studying the guanidinium hydrochloride-induced unfolding of the other, namely, that from *Trypanosoma cruzi* (TcTIM), appeared to be interesting. To this end, enzyme activity, far-UV circular dichroism, intrinsic and extrinsic fluorescence, and size-exclusion chromatography were monitored under equilibrium conditions. These data are consistent with the existence of two unfolding stable intermediates, namely, an expanded, non-native, and active dimer and a partially expanded monomer. The data allowed a complete thermodynamic characterization of the unfolding pathway that, in turn, is compared with those reported for TIMs from other species.

MATERIALS AND METHODS

Enzymes and Biochemicals. Guanidine hydrochloride (Gdn-HCl) was purchased from Boehringer GmbH Mannheim, and isopropyl β-D-thiogalactopyranoside was from GIBCO BRL. All other reagents were obtained from Sigma Chemical Co.

Overexpression and Purification of the Recombinant Protein. Escherichia coli BL21DE3 cells with the recombinant TcTIM gene were a generous gift of R. Pérez-Montfort (Instituto de Fisiología Celular, Universidad Nacional Autónoma de México). Overexpression and purification of TcTIM were performed as described by Ostoa-Saloma et al. (*37*). A single peak was obtained after chromatography, and the purified fractions exhibited a single band on a SDS−PAGE gel.

Enzyme Characterization. Absorbance measurements were carried out in a Beckman DU7500 spectrophotometer, with a cell compartment thermoregulated at 25 °C. Protein concentrations were determined either by the Lowry assay, using bovine serum albumin as the standard (*38*), or by measuring its absorbance at 280 nm using an absorption coefficient $A(280)^{1\%}_{1cm}$ of 1.33 calculated according to the method from ref *39*. TcTIM activity was followed by changes in absorbance at 340 nm due to oxidation of NADH in a coupled enzyme assay at 25 °C (*40*). Reaction conditions for the production of dihydroxyacetone phosphate were as follows: 100 mM triethanolamine, 10 mM EDTA, 1 mM dithiothreitol (TED 100/10/1) (pH 7.4), 1.5−3.0 mM D,L-glyceraldehyde 3-phosphate, 5−10 μg/mL α-glycerolphosphate dehydrogenase, and 0.2 mM NADH.

Reversibility. Reversibility was assayed as follows. Samples containing TcTIM (150 μg/mL) were incubated for 48 h at equilibrium at different Gdn-HCl concentrations. The highest Gdn-HCl concentration was 3.0 M, where complete denaturation is observed (see below). Renaturation was started by dilution of these samples with TED 100/10/1 (pH 7.4) to 5 μg of TcTIM/mL and either (i) a final (adjusted) Gdn-HCl concentration of 0.1 M or (ii) different residual (not adjusted) Gdn-HCl concentrations (see Figure 1). After 24 h, the catalytic activity was measured with 5 ng of TcTIM/mL.

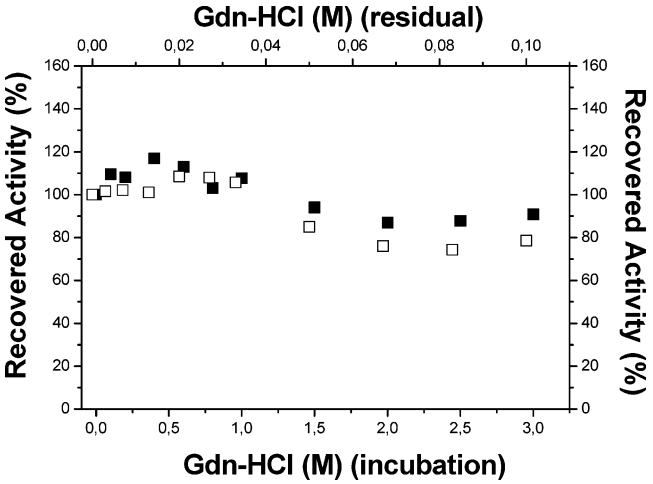

FIGURE 1: Refolding of TcTIM denatured in Gdn-HCl. The catalytic activity of TcTIM was measured 24 h after dilution of samples (150 μg/mL) equilibrated (48 h) at increasing Gdn-HCl concentrations (see Materials and Methods). Empty symbols represent data for refolding at variable residual Gdn-HCl concentrations and filled symbols refolding at 0.1 M Gdn-HCl.

Size-Exclusion Chromatography (SEC) and Determination of the Stokes Radius. SEC was performed in an FPLC system (Pharmacia, Uppsala, Sweden) using a Superdex 75 column as previously reported (*35*). The calibration curve was constructed using the experimentally determined elution volumes and the Stokes radii values reported for 10 proteins under native and denaturing conditions (*35*). The permeation properties of the Superdex 75 column are almost independent of Gdn-HCl concentration; thus, a single plot of elution volume versus Stokes radius (R_s) was built so that R_s can be easily obtained at each Gdn-HCl concentration (*35*). One hundred microliters of each sample [20 μg/mL in TED 100/10/1 (pH 7.4) at the respective concentration of Gdn-HCl in the same buffer] was injected into the column, previously equilibrated in the buffer with or without Gdn-HCl.

Guanidinium Hydrochloride Unfolding Experiments Monitored by Fluorescence and Circular Dichroism. In denaturation experiments, protein samples were incubated for equilibrium time (48 h) in TED 20/1/1 (pH 7.4) at 25 °C. The changes in fluorescence were monitored using an ISS PC1 photon counting spectrofluorometer (ISS, Champaign, IL) with the cell compartment thermoregulated at 25 °C. Protein intrinsic fluorescence was measured with an excitation wavelength of 280 or 295 nm (4.0 nm bandwidth); the emission was collected from 300−310 to 400−410 nm (4.0 nm bandwidth).

The far-UV circular dichroism changes were monitored with a JASCO J-715 spectropolarimeter following the change in ellipticity at 222 nm using cells with a path length of 0.1 cm thermoregulated at 25 °C. The values reported are the mean residue ellipticity recorded every 2 s for 4 min. Values obtained from reference samples at all denaturant concentrations that were studied were subtracted from all the spectroscopic measurements.

Determination of the Amount of Native Protein from Catalytic Activity Measurements. To avoid the effect of denaturants on α-glycerolphosphate dehydrogenase, the coupling enzyme in TIM activity measurements, samples previously used for CD or IF measurements were diluted in <1 min (final Gdn-HCl concentration of 60 mM), and

catalytic activity was measured immediately, following the method described in detail in refs *33* and *35*. This dilution is also necessary because catalytic activity measurements are carried out with 2.0 ng of TcTIM/mL, i.e., a concentration 2.5×10^4 times lower than that used for obtaining the denaturation patterns by spectroscopic probes.

ANS Fluorescence. 1-Anilino-8-naphthalenesulfonate (ANS) fluorescence was measured after excitation at 360 nm (4.0 nm bandwidth) in the 400−560 nm emission range. Saturating conditions (100 μM ANS) were obtained after titrations of the TcTIM samples with ANS (data not shown); thereafter, this saturating concentration was added to each sample and its corresponding blank solution under the same conditions mentioned above. Reference spectra with ANS at each Gdn-HCl concentration were subtracted from the spectra of the samples.

Data Analysis. The spectroscopic and activity data were analyzed according to a four-state equilibrium model involving a native homodimeric state (N_2), a non-native dimeric state (N_2*), a monomeric state (M), and an unfolded state (U):

$$N_2 \leftrightarrows N_2^* \leftrightarrows 2M \leftrightarrows 2U \quad (1)$$

Considering that the total mole concentration of protein is P_t:

$$P_t = 2[N_2] + 2[N_2^*] + [M] + [U] \quad (2)$$

the mole fractions of each species are

$$X_{N_2} = \frac{2[N_2]}{P_t},\ X_{N_2^*} = \frac{2[N_{2*}]}{P_t},\ X_M = \frac{[M]}{P_t},\ X_U = \frac{[U]}{P_t} \quad (3)$$

The sum of these mole fractions must equal unity

$$X_{N_2} + X_{N_2^*} + X_M + X_U = 1 \quad (4)$$

The equilibrium constants for the three transitions in eq 1 are

$$K_1 = \frac{[N_2^*]}{[N_2]} = \frac{X_{N_2^*}}{X_{N_2}},\ K_2 = \frac{[M]^2}{[N_2^*]} = \frac{2X_M{}^2 P_t}{X_{N_2^*}},\ K_3 = \frac{[U]^2}{[M]^2} = \frac{X_U{}^2}{X_M{}^2} \quad (5)$$

Using eqs 4 and 5, the following equation for X_M is obtained

$$X_M{}^2\left[\frac{2P_t(1+K_1)}{K_1K_2}\right] + X_M(1+K_3{}^{1/2}) - 1 = 0 \quad (6)$$

When quadratic equation (eq 6) is solved, the mole fractions of all species are obtained as

$$X_M = \frac{-(1+K_3{}^{1/2}) + \sqrt{(1+K_3{}^{1/2})^2 + 8P_t(1+K_1)/K_1K_2}}{4P_t(1+K_1)/K_1K_2} \quad (7)$$

$$X_{N_2^*} = \frac{2X_M{}^2 P_t}{K_2} \quad (8)$$

$$X_U = X_M K_3{}^{1/2} \quad (9)$$

$$X_{N_2} = 1 - X_{N_2^*} - X_M - X_U \quad (10)$$

Using the thermodynamic relation $K = \exp(-\Delta G/RT)$, eqs 7−10 can be expressed in terms of the Gibbs energy changes associated with the three transitions in eq 1. In turn, these ΔG values can be written as a function of denaturant concentration [d] assuming a linear dependence:

$$\Delta G_1 = \Delta G^o_{N_2 \leftrightarrow N_2^*} + m_1[d] \quad (11)$$

$$\Delta G_2 = \Delta G^o_{N_2^* \leftrightarrow 2M} + m_2[d] \quad (12)$$

$$\Delta G_3 = \Delta G^o_{2M \leftrightarrow 2U} + m_3[d] \quad (13)$$

where the ΔG^o values are the free energy changes in the absence of denaturant and m_1−m_3 are the cooperativity indices associated with each of the three transitions. The experimental observables, Y (fluorescence intensity or activity), are assumed to be additive

$$Y = Y_{N_2}X_{N_2} + Y_{N_2^*}X_{N_2^*} + Y_M X_M + Y_U X_U \quad (14)$$

where Y_Z values are the values of the observable for the respective Z species, estimated from the experimental data and kept as constants in the fitting procedure. To determine the unknown parameters $\Delta G^o_{N_2 \leftrightarrow N_2^*}$, $\Delta G^o_{N_2^* \leftrightarrow 2M}$, $\Delta G^o_{2M \leftrightarrow 2U}$, and m_1−m_3, fluorescence intensity and activity data were fitted using Origin 7.0.

RESULTS

Equilibrium Time. Equilibrium times for the unfolding transition of TcTIM were determined by following changes in intrinsic fluorescence. The change in the wavelength of maximal emission (λ_{max}), spectral center of mass (SCM), and intensity at native λ_{max} of samples incubated between 0 and 6.0 M Gdn-HCl indicated that the adequate time for equilibrium measurements is 48 h (data not shown). All the reported data belong to experiments previously equilibrated at this time.

Reversibility Assays. Samples of TcTIM were equilibrated at increasing Gdn-HCl concentrations from 0.1 to 3.0 M Gdn-HCl to equilibrium time (48 h) and subsequently diluted in buffer without denaturant to allow refolding. Their catalytic activity was determined after 24 h (Figure 1). In the refolding step, all samples contained 5 μg of TcTIM/mL and variable concentrations of residual Gdn-HCl (empty symbol) or a concentration of residual Gdn-HCl adjusted to 0.1 M (filled symbol) (see Materials and Methods). Samples preincubated at concentrations below 1.0 M Gdn-HCl in the unfolding step showed in both cases (variable or adjusted final Gdn-HCl concentration) the same or slightly higher activity compared to that of native TcTIM. High levels of renaturation (≈80%) were obtained in samples preincubated in more concentrated Gdn-HCl (Figure 1). Complete reversibility at a preincubation concentration of 6.0 M Gdn-HCl was previously reported (*41*).

Denaturation Pattern following Changes in Hydrodynamic Properties. To determine the denaturation pattern of TcTIM in Gdn-HCl, SEC−FPLC experiments were carried out at

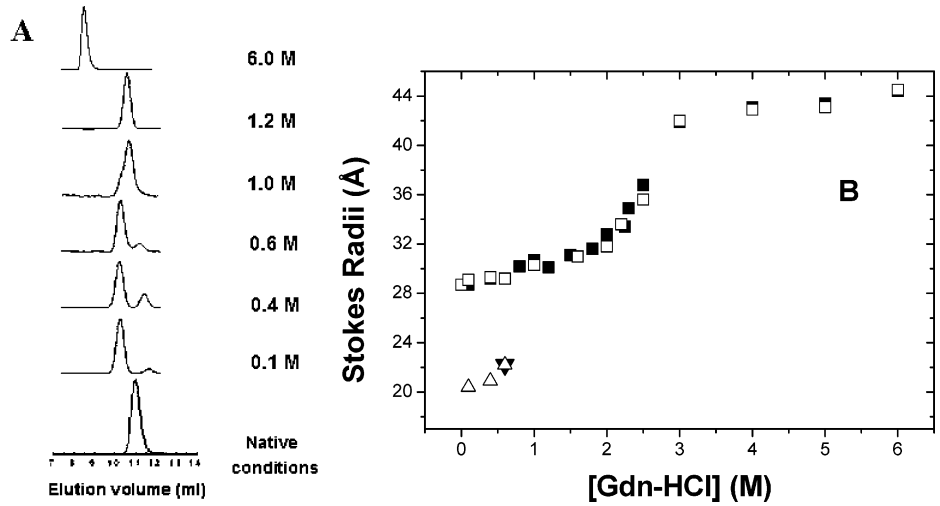

FIGURE 2: Denaturation pattern of TcTIM as a function of Gdn-HCl concentration. (A) Representative elution profiles of TcTIM equilibrated in Gdn-HCl. The chromatograms were obtained after equilibrium (48 h) of TcTIM samples (5 μg/mL) had been achieved at the indicated Gdn-HCl concentrations. Samples were then injected into a Superdex 75 column equilibrated at the same denaturant concentrations. (B) Change in the calculated Stokes radius as a function of Gdn-HCl concentration (see Materials and Methods). Filled and empty symbols correspond to 50 and 5 μg/mL TcTIM, respectively.

increasing concentrations of the denaturant. TcTIM samples at increasing Gdn-HCl concentrations were injected into a Superdex 75 column previously equilibrated at the same denaturant concentration according to the method from ref *35*. Figure 2A shows representative elution profiles of the denaturation of TcTIM. In the absence of denaturant, TcTIM exhibited a single peak in its elution profile. Between 0.1 and 0.6 M Gdn-HCl and at a TcTIM concentration of 5 μg/mL, two populations were observed (Figure 2A). At 0.8 (data not shown) and 1.0 M Gdn-HCl, only one peak was observed. At the latter concentration, the chromatogram is asymmetric, suggesting the presence of more than one species (Figure 2A). At 6.0 M Gdn-HCl, a single symmetric peak is observed. To obtain the change in Stokes radii as a function of denaturant concentration, the elution volumes were fitted according to method from ref *35*, and the denaturation profile was obtained (Figure 2B). The R_s value of native TcTIM is 28.7 Å, increasing to 44.4 Å at 6.0 M Gdn-HCl for the denatured protein (Figure 2B). Between 0.1 and 0.6 M Gdn-HCl, two different size populations coexist. One shows an increase of 2.0 Å in R_s with respect to the native R_s value. This increase in R_s might be indicative of the presence of a slightly more expanded dimer. The second population is observed at 0.1 M Gdn-HCl having an R_s value of 20 Å. It has been previously shown that this R_s value corresponds to a monomeric mutant of *T. brucei* TIM (TbTIM) (*35*). This observation strongly suggests that for the denaturation of TcTIM, there is also a monomeric intermediate. These two populations (□ and △ in Figure 2B) coexist only between 0.1 and 0.6 M denaturant. From 1.0 to 2.5 M Gdn-HCl, the R_s value (□ in Figure 2B) changes considerably from 30.7 to 36.8 Å. The same behavior is observed when the protein concentration is increased from 5 to 50 μg/mL (■ in Figure 2B), although for the latter the presence of two peaks is only observed at 0.6 M Gdn-HCl (▼ in Figure 2B). The explanation of the presence of a single peak is that a fast interconversion between states occurs, which is not detectable at 50 μg/mL in the chromatography experiment.

Changes in Tertiary Structure. As the Gdn-HCl concentration increases, the unfolding of TcTIM followed by fluorescence intensity (excitation at 280 and 295 nm) produced a nonmonophasic behavior (Figure 3), supporting data obtained by SEC about the presence of at least one folding intermediate. The region between 1.0 and 2.0 M Gdn-HCl is formed by a protein population with properties different from those of the native and denatured enzymes. In this region, approximately 60% of the fluorescence intensity is conserved and a clear plateau is observed (Figure 3). In the region between 0.1 and 1.0 M Gdn-HCl, a different behavior is observed for each of the two excitation wavelengths that were studied. At 280 nm, with respect to the signal in the absence of denaturant there is a significant increase in fluorescence intensity; at 295 nm, such an increase is not observed. No similar report has been made when studying

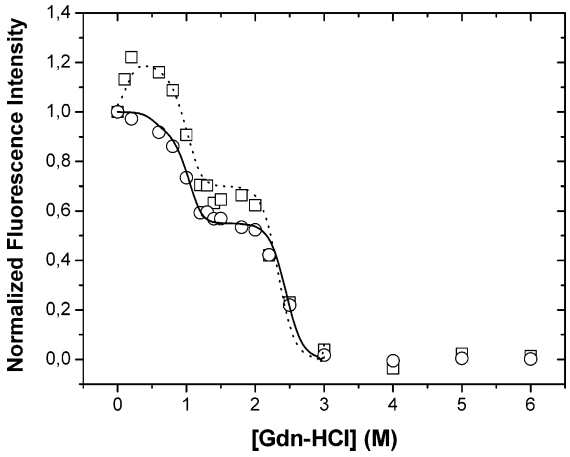

FIGURE 3: Changes in the intrinsic fluorescence intensity of TcTIM as a function of Gdn-HCl concentration. Intrinsic fluorescence intensity spectra of TcTIM (50 μg/mL) at the native λ_{max} were obtained after equilibrium had been achieved (48 h) at the indicated denaturant concentrations. The data were normalized using $[Y(d) - Y_U]/(Y_N - Y_U)$, where $Y(d)$ is the spectroscopic value at d (Gdn-HCl concentration) and Y_N and Y_U are the values for the native and unfolded TcTIM, respectively. Excitation wavelengths were 295 (○) and 280 nm (□). The lines correspond to the simultaneous fit of activity (see Figure 5) and intrinsic fluorescence intensity data (dotted line for excitation at 280 nm and solid line for 295 nm) from which the thermodynamic parameters were determined (see Table 1).

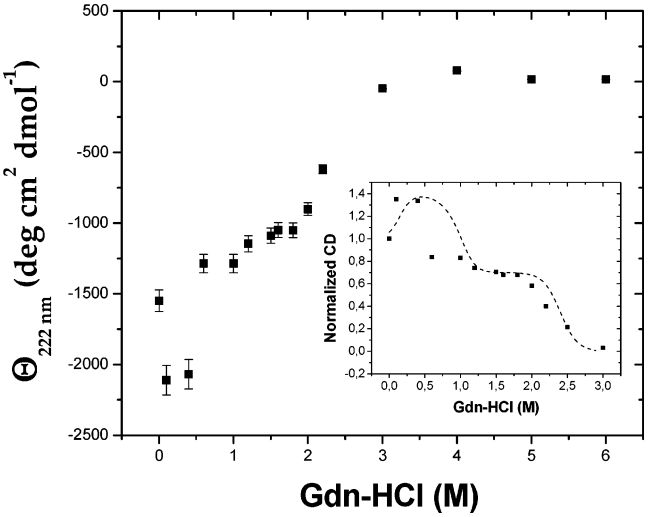

FIGURE 4: Changes in secondary structure of TcTIM as a function of Gdn-HCl concentration. The mean residue ellipticity values at 222 nm (θ_{222}) for TcTIM (50 μg/mL) were obtained after equilibrium had been achieved (48 h) at the indicated denaturant concentrations. The bars correspond to higher and lower values obtained in two different experiments. The symbols are the average of those two experiments. The inset shows normalized CD data using $[Y(d) - Y_U]/(Y_N - Y_U)$, where $Y(d)$ is the spectroscopic value at d (Gdn-HCl concentration) and Y_N and Y_U are the values for the native and unfolded TcTIM, respectively. The dotted line is the prediction using the parameters in Table 1 and the following values: $Y_{N_2} = 1$, $Y_{N_2*} = 1.4$, $Y_M = 0.7$, and $Y_U = 0$.

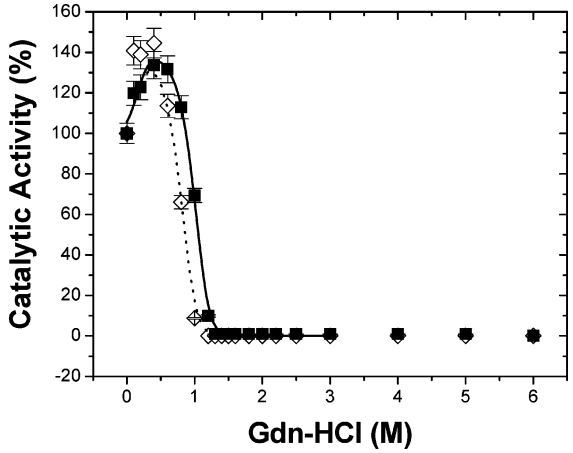

FIGURE 5: TcTIM catalytic activity as a function of Gdn-HCl concentration. Samples of TcTIM at 5 (◇) and 50 μg/mL (■) were incubated to equilibrium (48 h) at different concentrations of Gdn-HCl. Catalytic activity was measured as described in Materials and Methods; 100% is the activity of TcTIM in the absence of denaturant. The solid lines (undistinguishable) correspond to the simultaneous fit of activity and intrinsic fluorescence intensity data at 50 μg/mL (Figure 3) at 280 and 295 nm, respectively, from which the thermodynamic parameters were determined (Table 1). The dotted line corresponds to the predicted catalytic activity at 5 μg/mL TcTIM calculated using the parameters in Table 1.

the denaturation pattern of other TIMs. This behavior may be explained by either the effect of ionic strength on the fluorescence intensity or the change in the polar surroundings of the aromatic residues of the protein at these denaturant concentrations. The differences in fluorescence intensity results obtained at 280 and 295 nm are probably due to the global signal which includes tyrosine and tryptophan residues of the whole protein at 280 nm, and the more localized signal from tryptophan residues obtained at 295 nm. The nonmonophasic behavior displayed in Figure 3 is also observed at 5 μg/mL TcTIM.

Changes in Secondary Structure. The unfolding of TcTIM at equilibrium time in Gdn-HCl was also followed by far-UV circular dichroism (CD). Native TcTIM exhibits the characteristic CD spectra of β/α proteins (*41*). Changes in mean residue ellipticity at 222 nm are displayed in Figure 4. A nonmonophasic behavior was obtained with an increase in ellipticity between 0.1 and 0.4 M Gdn-HCl; in the region between 1.0 and 2.0 M denaturant, the ellipticity is constant (Figure 4), showing the same profile observed for fluorescence intensity (Figure 3). The increment in secondary structure in the denaturation pattern displayed in Figure 4 has not been reported for other TIMs. Both the increase in fluorescence intensity and CD at low denaturant concentrations and the presence of a plateau at higher Gdn-HCl concentrations strongly suggest the presence of two folding intermediates.

Changes in Quaternary Structure. Only TIM dimers are catalytically active; therefore, measurements of catalytic activity are equivalent to direct quantifications of the dimeric state or quaternary structure. Thus, activity measurements on the same samples shown in the previous figures quantify directly the mole fraction of native dimers. Two technical problems make the assessment of TIM catalysis under the conditions used for fluorescence and CD experiments difficult: (i) α-glycerol phosphate dehydrogenase, the coupling enzyme in TIM catalysis assays, is inactivated at high denaturant concentrations, and (ii) since TIM is a highly active enzyme, catalysis must be assessed at a concentration 4 orders of magnitude lower than those used in the spectroscopic experiments shown in Figures 3 and 4. However, these problems were circumvented by following the procedure described in Materials and Methods (see also ref *35*). At the same denaturant concentrations where fluorescence intensity and CD increased (Figures 3 and 4), an increase in catalytic activity is also observed (Figure 5). The same behavior has been reported in the denaturation of the enzyme of *Th. maritima* (TmTIM), although in this case the increase in activity is larger (80%), and no detectable alterations of both fluorescence emission and dichroic absorption were observed (*42*). The catalytic activity decreases sharply between 0.6 and 1.0 M Gdn-HCl, and in the region of 1.0−2.0 M Gdn-HCl, the denaturation pattern of TcTIM is formed by a nonactive population. The range of Gdn-HCl concentrations at which catalytic activity is completely lost includes the plateau region observed when following changes in tertiary and secondary structure (Figures 3 and 4; compare with Figure 5). The same global unfolding profile is observed at a TcTIM concentration of 5 or 50 μg/mL, but the denaturation pattern is shifted toward higher denaturant concentrations at the higher protein concentration. This is expected when a dissociation or bimolecular reaction is taking place (Figure 5).

Binding of the Fluorescent Dye. To further asses the existence and the properties of intermediates in the denaturation pattern, changes in ANS fluorescence (*43*) were recorded. Binding of ANS to predominantly hydrophobic segments is accompanied by a large increase in its fluorescence quantum yield (*43*−*46*). In samples equilibrated as in the aforementioned experiments, an increase in ANS fluorescence was evident in the interval between 1.0 and 2.5 M

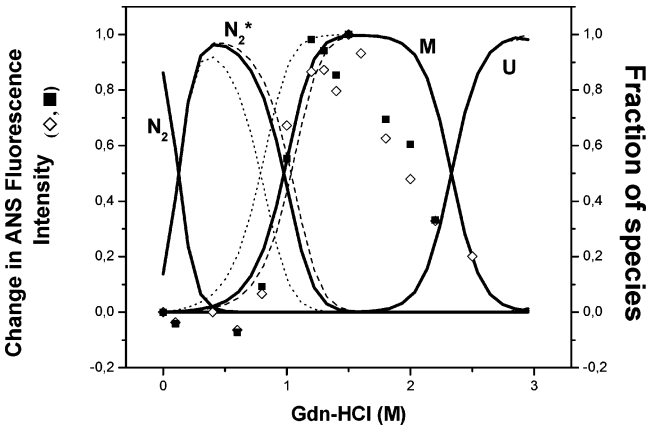

FIGURE 6: Binding of ANS to TcTIM as a function of Gdn-HCl concentration. TcTIM at 5 (◇) or 50 μg/mL (■) was equilibrated (48 h) at the indicated Gdn-HCl concentrations. Normalized ΔANS data (symbols) and the distribution of species (lines); the mole fractions of each species were calculated using the parameters in Table 1 (excitation at 280 nm) at different protein concentrations: 5 μg/mL (dotted line), 50 μg/mL (solid line), and 100 μg/mL (dashed line). N_2 is the native TcTIM dimer, N_2* the non-native dimer, M the monomer, and U the unfolded monomer.

Gdn-HCl (Figure 6). This Gdn-HCl concentration interval corresponds to the plateau observed for IF and CD (Figures 3 and 4) and to the region where catalytic activity is lost (Figure 5). The increment in the ANS fluorescence quantum yield is independent of protein concentration, with a maximum at 1.5 M Gdn-HCl.

DISCUSSION

In vitro irreversibility in the unfolding of oligomers is very frequent. TIM is not an exception, and aggregation has been reported in the unfolding of wild-type and monomeric mutants of TbTIM (*47*) induced by heat, of TIM from *Th. maritima* induced by either heat or Gdn-HCl (*42*), and of *P. falciparum* TIM (*30*) and *T. brucei* TIM (*35*) promoted by Gdn-HCl. Therefore, for these enzymes, it was not possible to analyze the denaturation pattern using standard thermodynamic models. In contrast, the Gdn-HCl-induced denaturation of TcTIM is reversible (Figure 1). Thus, it was possible to determine the thermodynamics of the transition between the homodimeric native enzyme and the denatured monomers.

Unfolding Pathway of TcTIM. Measurements at equilibrium of secondary, tertiary, and quaternary structures of TcTIM at various Gdn-HCl concentrations exhibit non-monophasic behavior. Two different intermediates appeared in the unfolding pathway, implying that a four-state model is required to describe TcTIM denaturation.

The first intermediate is observed at Gdn-HCl concentrations lower than 1.0 M. It is characterized by an increase in fluorescence intensity at an excitation wavelength of 280 nm (Figure 3) and in the secondary structure (Figure 4). This intermediate does not bind the fluorescent dye ANS, suggesting that hydrophobic regions of TcTIM are not exposed to the solvent (Figure 6). The nature of this intermediate is revealed by catalytic activity. Considering that only the dimers of TcTIM are catalytically active, this intermediate must be a non-native dimer that, in fact, exhibits higher activity (Figure 5). According to the SEC results in Figure 2B, this active non-native dimer possesses a slightly expanded structure (ΔR_s = 2.0 Å) relative to the native homodimer. The presence of dimeric intermediates has been previously observed in the denaturation pattern of *P. falciparum* (PfTIM) (*30*) and TbTIM (*35*). In these two TIMs, the global denaturing reaction is irreversible and the presence of a dimeric non-native intermediate is accompanied by off-pathway aggregates. Partially unfolded dimeric intermediates have also been reported in the Gdn-HCl-induced denaturation of other oligomeric proteins (*48*−*53*). The effect of Gdn-HCl as an activator agent of catalytic activity has been reported for TmTIM (*42*) and for other enzymes (*54*−*57*).

The second intermediate is detected between 1.0 and 2.0 M Gdn-HCl. At these denaturant concentrations, a plateau is observed using both spectroscopic fluorescence and CD techniques (Figures 3 and 4) where there is a complete loss of activity (Figure 5). This intermediate binds the fluorescent dye ANS, indicating that hydrophobic regions of TcTIM are exposed to the solvent (Figure 6). SEC results in Figure 2B show a species with an R_s value near 30 Å. Previous results with the monomeric TbTIM mutant RMMO-1 TIM show that the R_s of this mutant between 1.0 and 2.0 M Gdn-HCl has a value of 30 Å (*35*). All these observations suggest that in TcTIM denaturation this intermediate is an inactive expanded monomer. The presence of monomeric intermediates has been previously observed in the denaturation pattern of the yeast enzyme (yTIM) (*31*−*33*) and of the wild-type TbTIM (*35*).

Thermodynamic Parameters for TcTIM Unfolding. The simplest equilibrium process compatible with the obtained data is the four-state model described in Materials and Methods. The $N_2 \leftrightarrows N_2$* transition, dimer dissociation, and monomer unfolding are clearly reversible transitions (see Figures 1 and 5). To our knowledge, the four-state model has only been used to study the unfolding of Procaspase-3 (*58*). The model parameters were fitted in a simultaneous procedure to the fluorescence intensity and activity data at 50 μg/mL in Figures 3 and 5, giving the changes in Gibbs free energy reported in Table 1. The data are described well by the four-state model (see the lines in Figures 3 and 5). Using the parameters in Table 1, two predictions were made. The first was the prediction of the catalytic activity (at 5 μg/mL) and the amount of secondary structure (at 50 μg/mL) as a function of increasing Gdn-HCl concentrations. As seen in the inset of Figure 4 and in Figure 5, these predictions represent adequately the experimental data. The second prediction was the distribution of species (N_2, N_2*, M, and U) at different protein concentrations, displayed in Figure 6. Here, it is predicted that even at low Gdn-HCl concentrations (<1.0 M) monomers are present, in accordance with the experimental SEC results in Figure 2B; furthermore, the predicted maximum for the N_2* fraction coincides with the maximum activity in Gdn-HCl (compare Figures 5 and 6). Both these predictions confirm the soundness of the proposed model and the physical reliability of the obtained values for the parameters.

The bimolecular step in the unfolding pathway (from N_2* to 2M) must be dependent on protein concentration, and it must be seen in a narrow Gdn-HCl concentration range (0.5−1.5 M). The magnitude of this dependence depends on the thermodynamic parameters that describe the unfolding process (Table 1) and will be different for each property or observable (eq 14). Using the parameters in Table 1, the

Table 1: Thermodynamic Parameters for Gdn-HCl Equilibrium Denaturation of TcTIM[a]

	Y_{N_2}	Y_{N_2*}	Y_M	Y_U	$\Delta G^o_{N_2/N_2*}$	$\Delta G^o_{N_2*/2M}$	$\Delta G^o_{2M/2U}$	ΔG^o_{tot}
IF(λ_{max})295	1	0.95	0.55	0.0	4.3 ± 1.0	66.0 ± 2.2	37.9 ± 1.8	108.2
activity	1	1.4	0.0	0.0	(−26.8)	(−33.7)	(−15.5)	
IF(λ_{max})280	1	1.2	0.65	0.0	4.6 ± 1.2	65.6 ± 2.2	33.0 ± 2.7	103.2
activity	1	1.4	0.0	0.0	(−36.4)	(−33.2)	(−14.0)	
average					4.45 ± 1.1	65.8 ± 2.2	35.5 ± 2.3	105.7 ± 2.0

[a] Measurements were taken at 25 °C and pH 7.4. These parameters were obtained from the simultaneous fit of fluorescence intensity of TcTIM spectra at the native λ_{max} (excitation at 280 and 295 nm; see Figure 3) and activity data (Figure 5) to the model described in eq 1. Y_Z values are the amplitudes of the signals for the respective species (N_2, N_2*, M, and U), estimated from the experimental data and kept as constants during the fitting procedure. All the ΔG data are in kilojoules per mole, and m values (see eqs 11−13) are in parentheses.

Table 2: Analysis of the Unfolding of TIM in Gdn-HCl

Enzyme[a]	PDB Code[c]	Equil[d] Conds	REV	UP[e]	$C_{1/2}$	Δλ	AH in LGDN	Unfolding pathway [n]	IAB ANS	ΔG° (kJmol^{-1}) [o]	Ref.
BsTIM [b] [252/6.37]	1BTM [2.8]	24/25/8	Yes	nr[f]	nr	27[h,k]	no	$N_2 \rightarrow 2U$	-	101.3	**25**
TmTIM [b] [253/5.38]	1B9B [2.85]	48/variable/8	No	MP	3.5	16[i,k]	Yes	$N_2 \rightarrow A \rightarrow 2U$	-	-	**42**
rTIM [b] [248/6.89]	1R2R [1.5]	72/25/7.4 24/0/6.8	Yes	MP	0.55	19[i,j]	No	$N_2 \leftrightarrows 2U$	-	70 [60/5] 140.6	**27**,**28**, **29**
PfTIM [b] [248/6.37]	1YDV [2.2]	1/nr/8.0	No	NMP	nr	25[i,l,k]	No	$N_2 \rightarrow N_2* \rightarrow A \rightarrow 2U$	-	-	**30**
yTIM [b] [248/5.86]	1YPI [1.9]	24/25/7.4 24/25/7.2	Yes	MP NMP[g]	nr	30[i,k] 20[i,j]	No	$N_2 \leftrightarrows 2M \leftrightarrows 2U$	Yes	103.5 [70.3/16.6]	**31**,**32**, **33**
LmTIM [250/8.2]	1AMK [1.83]	12/20/7.5	Yes	MP	nr	25[m,k]	No	$N_2 \leftrightarrows 2U$	-	82.4	**34**
TbTIM [b] [250/9.85]	1TPF [1.8]	48/25/7.4	No	NMP	1.1, 2.2	20[l,j]	No	$\begin{matrix} & A & A \\ & \uparrow & \uparrow \\ N_2 & \leftrightarrows & N_2* \leftrightarrows 2M \leftrightarrows 2U \end{matrix}$	Yes	-	**35**
TcTIM [b] [251/8.19]	1TCD [1.83]	48/25/7.4	Yes	NMP	1.2, 2.4	21.4[i,j] 21.2[l,j] 35[i,k] 31.5[l,k]	Yes	$N_2 \leftrightarrows N_2* \leftrightarrows 2M \leftrightarrows 2U$	Yes	105.7	**This work**

[a] *BsTIM*, *B. stearothermophilus*; *TmTIM*, *Thermotoga maritima*; *rTIM*, rabbit; *PfTIM*, *P. falciparum*; *yTIM*, yeast [*S. cerevisiae*]; *LmTIM*, *L. mexicana*; *TbTIM*, *T. brucei*; *TcTIM*, *T. cruzi*. In brackets: number of total aminoacids by monomer and isoelectric point. [b] Recombinant enzyme obtained in *E. coli*. [c] Protein data bank code; in brackets is the resolution of the crystal (Å). [d] Equil Conds represents equilibrium conditions: time (hours)/temperature (degrees Celsius)/pH. [e] UP stands for unfolding pattern: followed by changes in secondary and/or tertiary structure and ^{1}H NMR (*32*). MP is monophasic, and NMP is nonmonophasic. [f] It must be monophasic. nr means not reported. [g] In renaturation. [h] Excitation at 290 nm. [i] Excitation at 280 nm. [j] Spectral center of mass. [k] Wavelength of maximal emission. [l] Excitation at 295 nm. [m] Excitation at 285 nm. [n] N_2 is the native dimer, N_2* the non-native dimer, M the folded monomer, U the unfolded monomer, and A the aggregate. [o] Reversibility. [p] In brackets are $\Delta G^o_{dissociation}/\Delta G^o_{monomer\ unfolding}$ values. [q] $C_{1/2}$ is the transition midpoint (M). [r] $\Delta\lambda$ is the total change in wavelength of maximal emission or the spectral center of mass upon complete dissociation or unfolding (nanometers). [s] AH in LGDN is the activity higher than for the native enzyme at low Gdn-HCl concentrations. [t] IABANS is whether the intermediate is able to bind ANS.

predicted dependences with protein concentration for fluorescence intensity and CD are quite small and hence difficult to determine; this is in fact what we experimentally observed at 5 and 50 μg/mL (data not shown). In contrast, for activity the expected shift is measurable (Figure 5).

Table 1 indicates that the total Gibbs energy change ΔG^o_{tot} for the transition between the native dimer (N_2) and the unfolded monomers (U) is large and similar to that for BsTIM and yTIM. The Gibbs energy associated with the transition between the native dimer (N_2) and the non-native active dimer (N_2*) is small (4.45 kJ/mol), accounting for only 4% of the ΔG^o_{tot}. Table 1 also shows that the energy change for the dissociation of the N_2* dimer ($\Delta G^o_{N_2*\leftrightarrow 2M}$ = 65.8 kJ/mol) is larger than that of monomer unfolding ($\Delta G^o_{M\leftrightarrow U}$ = 35.5/2 = 17.8 kJ/mol). This has been observed for all other TIM species for which these Gibbs energy changes have been evaluated (*33*). Hence, TcTIM subunit assembly also increases the conformational stability of the enzyme. However, for TcTIM this stabilization is less marked than that found in most TIMs from other species. This is clearly evidenced by the fractional contribution of monomer folding to the stability of the native enzyme (estimated as $-2\Delta G^o_{M\leftrightarrow U}/-\Delta G^o_{tot}$) that amounts to 0.34 for TcTIM, whereas for the other TIM species, it ranges from 0.14 for rabbit (rTIM) to 0.32 for yTIM (*33*). It appears that TcTIM monomers are more stable than those found for other TIM species (except yTIM), for which monomer stability is only marginal. Since this monomer binds ANS and possesses a considerable amount of both secondary and tertiary structure (see also refs *31*, *32*, and *35*), it could be considered a molten globule intermediate, similar to that reported for the unfolding of other proteins (*59*).

Equilibrium Unfolding of Homologous TIMs Induced by Gdn-HCl. The unfolding pathways induced by Gdn-HCl of TIMs from different species, together with a summary of relevant data regarding both the enzymes themselves and the unfolding process, are shown in Table 2. The reported equilibrium unfolding pathways differ in complexity, from a simple two-state process to multistate reactions that in some cases involve protein aggregation. More than 20 equilibrium and kinetic folding pathway studies of several homologous proteins can be found in the literature. The early studies indicate that the folding pathways of homologous proteins are similar, and that the folding of a certain conformation is conserved throughout evolution (*60*−*63*). However, there are examples of homologous proteins that unfold in different patterns (*64*−*73*). The more documented is TIM (Table 2). Despite the fact that the three-dimensional structures of oligomeric TIMs from different species are similar, their equilibrium unfolding pathways are different. Table 2 shows this heterogeneity: (i) two-state unfolding processes for *B. stearothermophilus* (BsTIM) (*25*), rabbit (rTIM) (*27*−*29*), and LmTIM (*34*), (ii) three-state processes involving a monomeric intermediate for *S. cerevisiae* (yTIM) (*31*−*33*) and involving aggregates for TmTIM (*42*), and (iii) a four-state process that involves a partially unfolded dimer which aggregates and unfolds in *P. falciparum* (PfTIM) (*30*), an irreversible aggregation of both a non-native dimer and a monomeric intermediate for *T. brucei* (TbTIM) (*35*), and the reversible unfolding pattern for TcTIM presented here. Among these unfolding profiles, those for TbTIM and TcTIM are particularly interesting because the level of identity in the primary structure for these two enzymes is greater than between the other studied TIMs. Of the 250 residues that are possible to compare (TcTIM possesses 251 and TbTIM 250), 185 of them (74%) are identical. In the remaining 26%, there are 30 conservative changes, which indicate that these enzymes possess only 13% nonconservative changes (*36*). Considering this small percentage of nonconserved residues, it is perhaps not surprising that TcTIM and TbTIM unfold following the same pathway that involves a non-native dimer and a partially expanded monomer intermediate, the difference being that for TbTIM the transitions are irreversible, due to the formation of aggregates.

ACKNOWLEDGMENT

We thank Laboratorio de Fisicoquímica y Diseño de Proteínas, Facultad de Medicina, Universidad Nacional Autónoma de México, and Dr. A. Gómez-Puyou and Dra. Marietta Tuena, IFC Universidad Nacional Autónoma de México, for generously making available their equipment facilities. We are grateful to Beatriz Aguirre and Nora Aguilar Ontiveros for their help in TcTIM purification and studies of TcTIM refolding, respectively. We also thank Dr. A. Gómez-Puyou and Dr. Rafael A. Zubillaga Luna for critically reading the manuscript.

REFERENCES

1. Blacklow, S. C., Raines, R. T., Lim, W. A., Zamore, P. D., and Knowles, J. R. (1988) Triosephosphate isomerase catalysis is difussion controlled, *Biochemistry 27*, 1158−1167.
2. Knowles, J. R., and Albery, W. J. (1977) Perfection in enzyme catalysis: The energetics of triosephosphate isomerase, *Acc. Chem. Res. 10*, 105−111.
3. Tellez-Valencia, A., Avila-Rios, S., Perez-Montfort, R., Rodriguez-Romero, A., Tuena de Gomez-Puyou, M., Lopez-Calahorra, F., and Gomez-Puyou, A. (2002) Highly specific inactivation of triosephosphate isomerase from *Trypanosoma cruzi*, *Biochem. Biophys. Res. Commun. 295*, 958−963.
4. Tellez-Valencia, A., Olivares-Illana, V., Hernandez-Santoyo, A., Perez-Montfort, R., Costas, M., Rodriguez-Romero, A., Lopez-Calahorra, F., Tuena de Gomez-Puyou, M., and Gomez-Puyou, A. (2004) Inactivation of triosephosphate isomerase from *Trypanosoma cruzi* by an agent that perturbs its dimer interface, *J. Mol. Biol. 341*, 1355−1365.
5. Walden, H., Bell, G. S., Russell, R. J. M., Siebers, B., Hensel, R., and Taylor, G. L. (2001) Tiny TIM: A small, tetrameric, hyperthermostable triosephosphate isomerase, *J. Mol. Biol. 306*, 745−757.
6. Maes, D., Zeelen, J. P., Thanki, N., Beaucamp, N., Alvarez, M., Dao Thi, M. H., Backmann, J., Martial, J. A., Wyns, L., Jaenicke, R., and Wierenga, R. K. (1999) The crystal structure of triosephosphate isomerase (TIM) from *Thermotoga maritima*: A comparative thermostability structural analysis of 10 different TIM structures, *Proteins 37*, 441−453.
7. Alvarez, M., Zeelen, J. P., Mainfroid, V., Rentier-Delrue, F., Martial, J. A., Wyns, L., Wierenga, R. K., and Maes, D. (1998) Triosephosphate isomerase (TIM) of the psychrophilic bacterium *Vibrio marinus*, *J. Biol. Chem. 273*, 2199−2206.
8. Noble, M. E. M., Zeelen, J. P., Wierenga, R. K., Mainfroid, V., Goraj, K., Gohimont, A. C., and Martial, J. A. (1993) Structure of triosephosphate isomerase from *Escherichia coli* determined at 2.6 Å resolution, *Acta Crystallogr. D49*, 403−417.
9. Delboni, L. F., Mande, S. C., Rentier-Delrue, F., Mainfroid, V., Turley, S., Vellieux, F. M. D., Martial, J. A., and Hol, W. G. J. (1995) Crystal structure of recombinant triosephosphate isomerase from *Bacillus stearothermophilus*. An analysis of potential thermostability factors in six isomerases with known three-dimensional structures points to the importance of hydrophobic interactions, *Protein Sci. 4*, 2594−2604.
10. Lolis, E., Alber, T., Davenport, R. C., Rose, D., Hartman, F. C., and Petsko, G. A. (1990) Structure of yeast triosephosphate isomerase at 1.9 Å resolution, *Biochemistry 29*, 6609−6618.
11. Wierenga, R. K., Noble, M. E. M., Vriend, G., Nauche, S., and Hol, W. G. J. (1991) Refined 1.83 Å structure of trypanosomal triosephosphate isomerase crystallized in the presence of 2.4 M ammonium sulphate. A comparison with the structure of the trypanosomal triosephosphate isomerase-glycerol-3-phosphate complex, *J. Mol. Biol. 220*, 995−1015.
12. Velanker, S. S., Ray, S. S., Gokhale, R. S., Suma, S., Balaram, H., Balaram, P., and Murthy, M. R. N. (1997) Triosephosphate isomerase from *Plasmodium falciparum*: The crystal structure provides insights into antimalarial drug design, *Structure 5*, 751−761.
13. Maldonado, E., Soriano-García, M., Moreno, A., Cabrera, N., Garza-Ramos, G., Tuena de Gómez-Puyou, M., Gómez-Puyou, A., and Pérez-Montfort, R. (1998) Differences in the intersubunit contacts in triosephosphate isomerase from two closely related pathogenic trypanosomes, *J. Mol. Biol. 283*, 193−203.
14. Williams, J. C., Zeelen, J. P., Neubauer, G., Vried, G., Backmann, J., Michels, P. A. M., Lambeir, A. M., and Wierenga, R. K. (1999) Structural and mutagenesis studies of *Leishmania* triosephosphate isomerase: A point mutation can convert a mesophilic enzyme into a superstable enzyme without losing catalytic power, *Protein Eng. 12*, 243−250.
15. Rodriguez-Romero, A., Hernandez-Santoyo, A., Del Pozo-Yauner, L., Kornhauser, A., and Fernandez-Velasco, D. A. (2002) Structure and inactivation of triosephosphate isomerase from *Entamoeba histolytica*, *J. Mol. Biol. 322*, 669−675.
16. Banner, D. W., Bloomer, A. C., Petsko, G. A., Phillips, D. C., Pogson, C. I., Wilson, I. A., Corran, P. H., Furth, A. J., Milman, J. D., Offord, R. E., Priddle, J. D., and Waley, S. G. (1975) Structure of chicken muscle triosephosphate isomerase determined crystallographically at 2.5 Å resolution using amino acid sequence data, *Nature 255*, 609−614.
17. Mande, S. C., Mainfroid, V., Kalk, K. H., Goraj, K., Martial, J. A., and Hol, W. G. (1994) Crystal structure of recombinant human triosephosphate isomerase at 2.8 Å resolution. Triosephosphate isomerase related human genetic disorders and comparison with the tripanosomal enzyme, *Protein Sci. 3*, 810−821.
18. Aparicio, R., Ferreira, S. T., and Polikarpov, I. (2003) Closed conformation of the active site loop of rabbit muscle triosephos-

phate isomerase in the absence of substrate: Evidence of conformational heterogeneity, *J. Mol. Biol. 334*, 1023−1041.
19. Kohlhoff, M., Dahm, A., and Hensel, R. (1996) Tetrameric triosephosphate isomerase from hyperthermophilic Archaea, *FEBS Lett. 383*, 245−250.
20. Farber, G. K., and Petsko, G. A. (1990) The evolution of α/β barrel enzymes, *Trends Biochem. Sci. 15*, 228−234.
21. Reardon, D., and Farber, G. K. (1995) The structure and evolution of α/β barrel proteins, *FASEB J. 9*, 497−503.
22. Brändén, C. I., and Tooze, J. (1991) *Introduction to protein structure*, Garland Publishing Inc., New York.
23. Knowles, J. R. (1991) Enzyme catalysis: Not different, just better, *Nature 350*, 121−124.
24. Wierenga, R. K., Noble, M. E. M., and Davenport, R. C. (1992) Comparison of the refined crystal structures of liganded and unliganded chicken, yeast and trypanosomal triosephosphate isomerase, *J. Mol. Biol. 224*, 1115−1126.
25. Mainfroid, V., Mande, S. C., Hol, W. G. J., Martial, J. A., and Goraj, K. (1996) Stabilization of human triosphosphate isomerase by improvement of the stability of individual α-helices in dimeric as well as monomeric forms of the protein, *Biochemistry 35*, 4110−4117.
26. Beaucamp, N., Hofmann, A., Kellerer, B., and Jaenicke, R. (1997) Dissection of the gene of the bifunctional PGK-TIM fusion protein from the hyperthermopilic bacterium *Thermotoga maritima*: Design and characterization of the separate triosephosphate isomerase, *Protein Sci. 6*, 2159−2165.
27. Rietveld, A. W., and Ferreira, S. T. (1996) Deterministic pressure dissociation and unfolding of triosephosphate isomerase: Persistent heterogeneity of a protein dimer, *Biochemistry 35*, 7743−7751.
28. Moreau, V. H., Rietveld, A. W. M., and Ferreira, S. T. (2003) Persistent conformational heterogeneity of triosephosphate isomerase: Separation and characterization of conformational isomers in solution, *Biochemistry 42*, 14831−14837.
29. Pan, H., Raza, A. S., and Smith, D. L. (2004) Equilibrium and kinetic folding of rabbit muscle triosephosphate isomerase by hydrogen exchange mass spectrometry, *J. Mol. Biol. 336*, 1251−1263.
30. Gokhale, R. S., Ray, S. S., Balaram, H., and Balaram, P. (1999) Unfolding of *Plasmodium falciparum* triosephosphate isomerase in urea and guanidinium chloride: Evidence for a novel disulfide exchange reaction in a covalently cross-linked mutant, *Biochemistry 38*, 423−431.
31. Vázquez-Contreras, E., Zubillaga, R., Mendoza-Hernández, G., Costas, M., and Fernández-Velasco, D. A. (2000) Equilibrium unfolding of yeast triosephosphate isomerase: A monomeric intermediate in guanidine-HCl and two-state behavior in urea. *Protein Pept. Lett. 7*, 57−64.
32. Morgan, C. J., Wilkins, D. K., Smith, L. J., Kawata, Y., and Dobson, C. M. (2000) A compact monomeric intermediate identified by NMR in the denaturation of dimeric triose phosphate isomerase, *J. Mol. Biol. 300*, 11−16.
33. Najera, H., Costas, M., and Fernandez-Velasco, D. A. (2003) Thermodynamic characterization of yeast triosephosphate isomerase refolding: Insights into the interplay between function and stability as reasons for the oligomeric nature of the enzyme, *Biochem. J. 370*, 785−792.
34. Lambeir, A. M., Backmann, J., Ruiz-Sanz, J., Filimonov, V., Nielsen, J. E., Kursula, I., Norledge, B. V., and Wierenga, R. K. (2000) The ionization of a buried glutamic acid is thermodynamically linked to the stability of *Leishmania mexicana* triose phosphate isomerase, *Eur. J. Biochem. 267*, 2516−2524.
35. Chánez-Cárdenas, M. E., Fernández-Velasco, D. A., Vázquez-Contreras, E., Coria, R., Saab-Rincón, G., and Pérez Montfort, R. (2002) Unfolding of triosephosphate isomerase from *Trypanosoma brucei*: Identification of intermediates and insight into the denaturation pathway using tryptophan mutants, *Arch. Biochem. Biophys. 399*, 117−129.
36. Chánez-Cárdenas, M. E., and Vázquez-Contreras, E. (2002) Two notably similar proteins follow different unfolding pathways. *Rev. Soc. Quim. Mex. 46*, 219−222.
37. Ostoa-Saloma, P., Garza-Ramos, G., Ramírez, J., Becker, I., Berzunza, I., Landa, A., Gómez-Puyou, A., Tuena de Gómez-Puyou, M., and Pérez-Montfort, R. (1997) Cloning, expression, purification and characterization of triosephosphate isomerase from *Trypanosoma cruzi*, *Eur. J. Biochem. 244*, 700−705.
38. Lowry, O. H., Rosebrough, N. J., Farr, A. L., and Randall, R. J. (1951) Protein measurement with the Folin phenol reagent, *J. Biol. Chem. 193*, 265−275.
39. Pace, C. N., Vajdos, F., Fee, L., Grimsley, G., and Gray, T. (1995) How to measure and predict the molar absorption coefficient of a protein, *Protein Sci. 4*, 2411−2423.
40. Rozacky, E. E., Sawyer, T. H., Barton, R. A., and Gracy, R. W. (1971) Studies on human triosephosphate isomerase. I. Isolation and properties of the enzyme from erythrocytes, *Arch. Biochem. Biophys. 146*, 312−320.
41. Zomosa-Signoret, V., Hernández-Alcántara, G., Reyes-Vivas, H., Martínez-Martínez, E., Garza-Ramos, G., Pérez-Montfort, R., Tuena de Gómez-Puyou, M., and Gómez-Puyou, A. (2003) Control of the reactivation kinetics of homodimeric triosephosphate isomerase from unfolded monomers, *Biochemistry 42*, 3311−3318.
42. Beaucamp, N., Hofmann, A., Kellerer, B., and Jaenicke, R. (1997) Dissection of the gene of the bifunctional PGK-TIM fusion protein from the hyperthermopilic bacterium *Thermotoga maritima*: Design and characterization of the separate triosephosphate isomerase. *Protein Sci. 6*, 2159−2165.
43. Rosen, C. G., and Weber, G. (1969) Dimer formation from 1-amino-8-naphthalenesulfonate catalyzed by bovine serum albumin. A new fluorescent molecule with exceptional binding properties, *Biochemistry 8*, 3915−3920.
44. Ptitsyn, O. B., Pain, R. H., Semisotnov, G. V., Zerovnik, E., and Razgulyaev, O. I. (1990) Evidence for a molten globule state as a general intermediate in protein folding, *FEBS Lett. 262*, 20−24.
45. Semisotnov, G. V., Rodionova, N. A., Razgulyaev, O. I., Uversky, V. N., Gripas, A. F., and Gilmanshin, R. I. (1991) Study of the "molten globule" intermediate state in protein folding by a hydrophobic fluorescent probe, *Biopolymers 31*, 119−128.
46. Silva, J. L., Silveira, C. F., Correia, A., Jr., and Pontes, L. (1992) Dissociation of a native dimer to a molten globule monomer. Effects of pressure and dilution on the association equilibrium of arc repressor, *J. Mol. Biol. 223*, 545−555.
47. Schliebs, W., Thanki, N., Jaenicke, R., and Wierenga, R. K. (1997) A double mutation at the tip of the dimer interface loop of triosephosphate isomerase generates active monomers with reduced stability, *Biochemistry 36*, 9655−9662.
48. Teschner, W., and Garel, J. R. (1989) Intermediates on the reassociation pathway of phosphofructokinase I from *Escherichia coli*, *Biochemistry 28*, 1912−1916.
49. Plomer, J. J., and Gafni, A. (1992) Denaturation of glucose-6-phosphate dehydrogenase from *Leuconostoc mesenteroides* by guanidine hydrochloride: Identification of inactive, partially unfolded, dimeric intermediates. *Biochim. Biophys. Acta 1122*, 234−242.
50. Plomer, J. J., and Gafni, A. (1993) Renaturation of glucose-6-phosphate dehydrogenase from *Leuconostoc mesenteroides* after denaturation in 4 M guanidine hydrochloride: Kinetics of aggregation and reactivation, *Biochim. Biophys. Acta 1163*, 89−96.
51. Mei, G., Di Venere, A., Buganza, M., Vecchini, P., Rosato, N., and Finazzi-Agro, A. (1997) Role of quaternary structure in the stability of dimeric proteins: The case of ascorbate oxidase, *Biochemistry 36*, 10917−10922.
52. Grimsley, J. K., Scholtz, J. M., Pace, C. N., and Wild, J. R. (1997) Organophosphorus hydrolase is a remarkably stable enzyme that unfolds through a homodimeric intermediate, *Biochemistry 36*, 14366−14374.
53. Li, X. L., Lei, X. D., Cai, H., Li, J., Yang, S. L., Wang, C. C., and Tsou, C. L. (1998) Binding of a burst-phase intermediate formed in the folding of denatured D-glyceraldehyde-3-phosphate dehydrogenase by chaperonin 60 and 8-anilino-1-naphthalenesulphonic acid, *Biochem. J. 331* (Patt 2), 505−511.
54. Rao, N. M., and Nagaraj, R. (1991) Anomalous stimulation of *Escherichia coli* alkaline phosphatase activity in guanidinium chloride. Modulation of the rate-limiting step and negative cooperativity, *J. Biol. Chem. 266*, 5018−5024.
55. Fernández-Velasco, D. A., Garza-Ramos, G., Ramírez, L., Shoshani, L., Darzon, A., Tuena de Gómez-Puyou, M., and Gómez-Puyou, A. (1992) Activity of heart and muscle lactate dehydrogenases in all-aqueous systems and in organic solvents with low amounts of water. Effect of guanidine chloride, *Eur. J. Biochem. 205*, 501−508.
56. Garza-Ramos, G., Fernández-Velasco, D. A., Ramírez, L., Shoshani, L., Darzon, A., Tuena de Gómez-Puyou, M., and Gómez-Puyou, A. (1992) Enzyme activation by denaturants in organic solvent systems with a low water content, *Eur. J. Biochem. 205*, 509−517.

57. Tuena de Gómez-Puyou, M., Domínguez-Ramírez, L., Reyes-Vivas, H., and Gómez-Puyou, A. (2001) Structural alterations and inhibition of unisite and multisite ATP hydrolysis in soluble mitochondrial F1 by guanidinium chloride, *Biochemistry 40*, 3396−3402.
58. Bose, K., and Clark, A. C. (2001) Dimeric procaspase-3 unfolds via a four-state equilibrium process, *Biochemistry 40*, 14236−14242.
59. Ptitsyn, O. B. (1992) The molten globule state, in *Protein Folding* (Creigthon, T. E., Ed.) pp 243−255, Freeman, New York.
60. Hollecker, M., and Creighton, T. E. (1983) Evolutionary conservation and variation of protein folding pathways. Two protease inhibitor homologues from black mamba venom, *J. Mol. Biol. 168*, 409−437.
61. Krebs, H., Schmid, F. X., and Jaenicke, R. (1983) Folding of homologous proteins. The refolding of different ribonucleases is independent of sequence variations, proline content and glycosylation, *J. Mol. Biol. 169*, 619−635.
62. Stackhouse, T. M., Onuffer, J. J., Matthews, R., Ahmed, S. A., and Miles, E. W. (1988) Folding of homologous proteins: Conservation of the folding mechanisms of the α subunit of tryptophan synthase from *Escherichia coli*, *Salmonella typhimurium*, and five interspecies hybrids, *Biochemistry 27*, 824−832.
63. Kragelund, B. B., Hojrup, P., Jensen, M. S., Schjerling, C. K., Juul, E., Knudsen, J., and Poulsen, F. M. (1996) Fast and one-step folding of closely and distantly related homologous proteins of a four-helix bundle family, *J. Mol. Biol. 256*, 187−200.
64. Chang, J. Y. (1996**)** The Disulfide Folding Pathway of Tick Anticoagulant Peptide (TAP), a Kunitz-Type Inhibitor Structurally Homologous to BPTI, *Biochemistry 35*, 11702−11709.
65. Plaxco, K. W., Spitzfaden, C., Campbell, I. D., and Dobson, C. M. (1997) A comparison of the folding kinetics and thermodynamics of two homologous fibronectin type III modules, *J. Mol. Biol. 270*, 763−770.
66. Zerovnik, E., Virden, R., Jerala, R., Turk, V., and Waltho, J. P. (1998) On the mechanism of human stefin B folding. I. Comparison to homologous stefin A. Influence of pH and trifluoroethanol on the fast and slow folding phases, *Proteins 32*, 296−303.
67. Ferguson, N., Capaldi, A. P., James, R., Kleanthous, C., and Radford, S. E. (1999) Rapid folding with and without populated intermediates in the homologous four-helix proteins Im7 and Im9, *J. Mol. Biol. 286*, 1597−1608.
68. Widmann, M., and Christen, P. (2000) Comparison of folding rates of homologous prokaryotic and eukaryotic proteins, *J. Biol. Chem. 275*, 18619−18622.
69. Tieman, B. C., Johnston, M. F., and Fisher, M. T. (2001) A comparison of the GroE chaperonin requirements for sequentially and structurally homologous malate dehydrogenases: The importance of folding kinetics and solution environment, *J. Biol. Chem. 276*, 44541−44550.
70. Srimathi, T., Kumar, T. K., Kathir, K. M., Chi, Y. H., Srisailam, S., Lin, W. Y., Chiu, I. M., and Yu, C. (2003) Structurally homologous all *β*-barrel proteins adopt different mechanisms of folding, *Biophys. J. 85*, 459−472.
71. Ichimaru, T., and Kikuchi, T. (2003) Analysis of the differences in the folding kinetics of structurally homologous proteins based on predictions of the gross features of residue contacts, *Proteins 51*, 515−530.
72. Friel, C. T., Capaldi, A. P., and Radford, S. E. (2003) Structural analysis of the rate-limiting transition states in the folding of Im7 and Im9: Similarities and differences in the folding of homologous proteins, *J. Mol. Biol. 326*, 293−305.
73. Fitter, J., and Haber-Pohlmeier, S. (2004) Structural stability and unfolding properties of thermostable bacterial α-amylases: A comparative study of homologous enzymes, *Biochemistry 43*, 9589−9599.

BI047687A